

Kaon and pion femtoscopy at the highest energies available at the BNL Relativistic Heavy Ion Collider (RHIC) in a hydrokinetic model

Iu.A. Karpenko, Yu.M. Sinyukov

*Bogolyubov Institute for Theoretical Physics,
Metrolohichna str. 14b, 03680 Kiev, Ukraine*

Abstract

The hydrokinetic approach, that incorporates hydrodynamic expansion of the systems formed in A+A collisions and their dynamical decoupling, is applied to restore the initial conditions and space-time picture of the matter evolution in central Au+Au collisions at the top RHIC energy. The analysis is based on the detailed reproduction of the pion and kaon momentum spectra and femtoscopic data in whole interval of the transverse momenta studied by both STAR and PHENIX collaborations. The fitting procedure utilizes the two parameters: the maximal energy density at supposed thermalization time 1 fm/c and the strength of the pre-thermal flows developed to this time. The quark-gluon plasma and hadronic gas is supposed to be in complete local equilibrium above the chemical freeze-out temperature $T_{ch} = 165$ MeV with the equation of states (EoS) at high temperatures as in the lattice QCD. Below T_{ch} the EoS in the expanding and gradually decoupling fluid depends on the composition of the hadron-resonance gas at each space-time point and accounts for decays of resonances into the non-equilibrated medium. A good description of the pion and kaon transverse momentum spectra and interferometry radii is reached at both used initial energy density profiles motivated by the Glauber and Color Glass Condensate (CGC) models, however, at different initial energy densities. The discussion as for the approximate pion and kaon m_T -scaling for the interferometry radii is based on a comparison of the emission functions for these particles.

PACS numbers: 25.75.-q, 25.75.Cj, 25.75.Ld

I. INTRODUCTION

At present the majority of the dynamical models of A+A collisions, which describe the soft physics phenomena are based on the Landau's idea [1] of space-time evolution of the thermal matter formed in the collisions. This approach implies at once the specific space-time scales in the problem of nuclear scattering such as a time of expansion, a volume occupied by the fireball, hydrodynamic lengths, etc. The only direct tool to measure these femtoscopic scales is the intensity interferometry method, often called now as the femtoscopy. The measured scales - the interferometry, or HBT radii - are associated just with the homogeneity lengths in the rapidly expanding system created in heavy ion collisions [2]. So, the comparison with experimental data of the space-time scales characterizing such and such dynamical model of the system evolution and particle production should be one of the first task of a justification of the model and discrimination between different approaches. Nevertheless, such a comparison was often ignored since almost all dynamic models, which pretend to be complete and therefore describe the evolution of the matter as well as its gradual decay, e.g., the hybrid (hydrodynamic plus UrQMD) models [3] failed to reproduce pion out-, side-, long- interferometry radii simultaneously with the hadronic spectra at RHIC. Until now it was possible to reach only when some artificial parametrization of freeze-out processes, e.g. a sudden freeze-out at a fairly large temperature close to the hadronization one [4], is utilized.

In Refs. [5–7] the HydroKinetic Model (HKM) for A+A collisions has been developed. It combines the advantages of the hydrodynamic approximation, where possible phase transitions are encoded in the corresponding equation of state (EoS), and microscopic approach, accounting for a non-equilibrated process of the spectra formation due to gradual particle liberation. The dynamical decoupling is described by the particle escape probabilities in inhomogeneous hydrodynamically expanding systems in the way consistent with the kinetic equations in the relaxation time approximation for emission function [5]. The method can be applied to match correctly hydrodynamics and UrQMD using as the input the locally non-equilibrated distribution functions from the HKM. Then one can match these models at space-like hypersurfaces related to the late stage of the evolution, escaping thus the inconsistencies connected with an inapplicability of hadron cascade models at very high densities and with the causality [8].

The HKM method also allows one to take into account a back reaction of particle emission on the hydrodynamic evolution that corresponds an account of the viscous effects at the hadronic stage of the evolution [6]. It is worth noting that found in the HKM ratio of the shear viscosity to the total entropy is less than 1/2 in the space-time region of maximal hadronic emission [9]. An analysis of the QGP evolution within viscous hydrodynamics is also a topical problem since the shear viscosity brings an important effect, an increase of transverse flows during the evolution [10]. However, until the viscosity of the QGP as the function of the temperature becomes clear, this effect is simpler to take into account in the phenomenological way, as it is proposed in what follows.

In this article we apply the HydroKinetic Model (HKM) [5, 6] to an analysis of the femtoscopic measurements at RHIC for central Au+Au collisions at the top energy $\sqrt{s} = 200$ AGeV. Namely, we analyze pion and kaon transverse momentum spectra and the m_T -behavior of the pion and kaon interferometry radii to clarify, in particular, how these observables depend on the initial conditions: Glauber and CGC-like. The basic hydrokinetic code, proposed in [6], is modified now to include decays of resonances into the expanding hadronic chemically non-equilibrated system and, based on the resulting composition of the hadron-resonance gas at each space-time point, to calculate the equation of state (EoS) in a vicinity of this point. The obtained local EoS allows one to determine the further evolution of the considered fluid elements. In the zone of chemical equilibrium, above the chemical freeze-out temperature, the EoS is taken in accordance with the lattice QCD results.

The paper is organized as the following. Section II is devoted to the initial conditions (IC) for thermal evolution of the matter in Au+Au collisions at RHIC. In Section III we discuss the EoS of the matter in equilibrated and chemically non-equilibrated zones. The kinetics of the system in the non-equilibrium zone related to system's evolution and decoupling is described in Section IV. The underlying hydrodynamic model for both chemically equilibrated and non-equilibrated domains is presented in Section V. Section VI is devoted to the results obtained and discussions. The conclusions and outlook are done in Section VII.

II. INITIAL CONDITIONS FOR HYDRO-EVOLUTION OF THERMAL MATTER

Our results are all related to the central rapidity slice where we use the boost-invariant Bjorken-like initial condition in longitudinal direction. We consider the proper time of thermalization of quark-gluon matter as the minimal one discussed in the literature, $\tau_0 = 1$ fm/c [11].

A. Pre-thermal flows

If one starts the hydrodynamic evolution at the "conventional time" $\tau_i = 1$ fm/c *without* transverse flow - since no pressure is established before thermalization - the resulting radial flow will not be developed enough to describe simultaneously the absolute values of pion, kaon and proton spectra, as well as the anisotropy of elliptic flow in non-central collisions. To describe the observables one needs to start the hydro-evolution at very small initial time, $\tau \sim 0.5$ fm/c [12], where it is difficult to expect the thermalization. This controversial situation is overcome due to the results of Ref. [13] where is shown that the initial transverse flows in thermal matter as well as their anisotropy, leading to asymmetry of the transverse momentum spectra in non-central collisions, could be developed at the pre-thermal, either classical field (Glasma) [14], string [15] or partonic stages, with even more efficiency than in the case of very early hydrodynamics. So, the hypotheses of early thermalization at times less than 1 fm/c is not necessary: the radial and elliptic flows develop no matter whether a pressure already established. The general reason for them is an essential finiteness of the system in transverse direction. Then the flows of particle number or energy directed outward the system cannot be compensated by the inward directed (from periphery to the centre) flows. This difference means the non-zero net flows no matter how the collective velocity is defined: according to Ekkart or to Landau-Lifshitz. The further development and exploitation of these results were done in Refs. [16–18].

The initial transverse rapidity profile is supposed to be linear in radius r_T :

$$y_T = \alpha \frac{r_T}{R_T}, \quad \text{where} \quad R_T = \sqrt{\langle r_T^2 \rangle}, \quad (1)$$

here α is the second fitting parameter. Note that the fitting parameter α should include also a positive correction for underestimated resulting transverse flow since in this work we did not account in direct way for the viscosity effects [10] neither at QGP stage nor at hadronic

one. In formalism of HKM [6] the viscosity effects at hadronic stage are incorporated in the mechanisms of the back reaction of particle emission on hydrodynamic evolution which we ignore in current calculations. Since the corrections to transverse flows which depend on unknown viscosity coefficients are unknown, we use fitting parameter α to describe the "additional unknown portions" of flows, caused both factors: by a developing of the pre-thermal flows and the viscosity effects in quark-gluon plasma.

B. Glauber-like initial transverse profile

A simple Glauber model initialization assumes that the initial energy density in the transverse plane is proportional to the participant nucleon density [19],

$$\epsilon(\mathbf{b}, \mathbf{x}_T) = \epsilon_0 \frac{\rho(\mathbf{b}, \mathbf{x}_T)}{\rho_0} \quad (2)$$

with $\rho_0 \equiv \rho(0, 0)$ and

$$\begin{aligned} \rho(\mathbf{b}, \mathbf{x}_T) &= (T(\mathbf{x}_T + \mathbf{b}/2)S(\mathbf{x}_T - \mathbf{b}/2) + T(\mathbf{x}_T - \mathbf{b}/2)S(\mathbf{x}_T + \mathbf{b}/2)), \\ S(\mathbf{x}_T) &= \left[1 - \left(1 - \sigma_{NN} \frac{T(\mathbf{x}_T)}{A} \right)^A \right], \end{aligned} \quad (3)$$

where A is atomic number, equal to 197 for Au+Au collision, and $\sigma_{NN} = 51 \text{ mb} (= 5.1 \text{ fm}^2)$ is the nucleon-nucleon cross-section at $\sqrt{s_{NN}} = 200 \text{ AGeV}$. The impact parameter $\mathbf{b} = (b, 0)$ is equal to zero, $b=0$, in the considered case of central collision. The parameter $\epsilon_0 \equiv \epsilon(b = 0, \mathbf{x}_T = 0)$ is the maximal energy density at the initial moment of thermalization. The thickness $T(\mathbf{x}_T)$ is expressed through the Woods-Saxon distribution profile:

$$T(\mathbf{x}_T) = \int_{-\infty}^{\infty} F_{\text{WS}}(\mathbf{x}) dx_L, \quad (4)$$

where

$$F_{\text{WS}}(\mathbf{x}) = \frac{a}{\exp \left[\left(\sqrt{x_L^2 + x_T^2} - R_A \right) / \delta \right] + 1}. \quad (5)$$

Here we use that $R_A = 1.12A^{1/3} - 0.86A^{-1/3} \approx 6.37 \text{ fm}$, $\delta = 0.54 \text{ fm}$. Constant a is obtained from normalization condition:

$$\int T(\mathbf{x}_T) d^2 x_T = A. \quad (6)$$

One can think that transversal Glauber-like ϵ -profile has been formed to some initial time $\tau_0 \approx 0.1 - 0.3$ fm/c (see below) when the system is not thermal yet. However, the form of the profile is, practically, not modified to supposed thermalization time $\tau_0 \sim 1$ fm/c because the transverse velocities reached to this time are relatively small. At the same time, the absolute values of energy density can change significantly because of the strong longitudinal expansion. We use the maximal energy density ϵ_0 at time $\tau_i = 1$ fm/c as the second fitting parameter.

C. Initial conditions motivated by Color Glass Condensate model

Within CGC effective field theory some important physical properties of the field are defined by the parameter $\Lambda_s = g^2 \mu$ where $g^2 = 4\pi\alpha_s$ and μ^2 is dimensionless parameter, which is the variance of the Gaussian weight over the color charges ρ of partons. The value of Λ_{s0} is approximately equal to the saturation scale value, Q_s , and for the RHIC energies one can use $\Lambda_{s0} \approx Q_s \approx 2$ GeV² [20]. According to the results of Refs. [21, 22], (proper) time $\tau_0 \approx 3/\Lambda_s$ is an appropriate scale controlling the formation of gluons with a physically well-defined energy. At later times the dynamics of the classical Yang- \tilde{U} -Mills fields produced in nucleus-nucleus collisions can be linearized and approximated by that of a system of weakly coupled harmonic oscillators. Then one can compute the field amplitudes squared in momentum space and find corresponding distribution for the gluon number [22, 23] for cylindrically homogeneous transverse profile. It has the form at $p_T < 1.5\Lambda_s$ and $\eta = \frac{1}{2} \ln \frac{t+x_L}{t-x_L} \simeq 0$,

$$\begin{aligned} \frac{dN}{d^2p_T d^2x_T d\eta} &\equiv f(T_{\text{eff}}) \\ &= \frac{a_1}{g^2} \left[\exp \left(\sqrt{p_T^2 + m_{\text{eff}}^2} / T_{\text{eff}} \right) - 1 \right]^{-1}, \end{aligned} \quad (7)$$

where $m_{\text{eff}} = a_2\Lambda_{s0}$, $T_{\text{eff}} = a_3\Lambda_s$; $a_2 = 0.0358$, $a_3 = 0.465$. The constant a_1/g^2 will be absorbed into factor ϵ_0 which is our fitting parameter.

The dependence of the distribution (7) on transverse coordinates \mathbf{x}_T is constructed as follows [22]:

$$\Lambda_s^2(\mathbf{x}_T) = \Lambda_{s0}^2 \frac{\rho(\mathbf{b}, \mathbf{x}_T)}{\rho_0}. \quad (8)$$

where the participant density at a particular position in the transverse plane is defined by (3).

To define the initial energy density profile we need the partonic phase-space distribution $f_0(x, p) = dN/d^3x d^3p$. Note, that it is associated with the hypersurfaces $t = \text{const.}$ To express the phase-space density through the values $\frac{dN}{d^2x_T d^2p d\eta}$ defined at $\sqrt{t^2 - x_L^2} = \tau_0$, one should take into account that the density of partons with momentum \mathbf{p} crossing element $d^3\sigma(x)$ of this hypersurface is

$$\begin{aligned} p^0 \frac{dN}{d^3p} \Big|_{d\sigma(x)} &= p^\mu d\sigma_\mu(x) f_0(x, p) \\ &= f_0(x, p) \tau_0 p_T \cosh \theta d^2x_T d\eta, \end{aligned} \quad (9)$$

where $\theta = y - \eta$, y is rapidity of partons (in momentum space). Therefore

$$f_0(x, p) = \frac{1}{\tau_0 m_T \cosh \theta} \frac{dN}{d^2x_T d^2p_T d\eta dy}. \quad (10)$$

One can formally get the d^6N distribution from (7) by multiplying it by δ -function:

$$\frac{dN}{d^2p_T d^2x_T d\eta dy} = f(T_{\text{eff}}) \delta(y - \eta). \quad (11)$$

Such a phase-space distribution, corresponding the CGC asymptotic results [24], is widely used for a description of the initial state in A+A collisions [25]. However, a presence of the delta-function in the phase-space density contradicts evidently to the basic principle of the quantum mechanics. Indeed, the classical phase-space density has to follow from the quantum mechanical one in some limit. The Wigner function $f_W(x, p)$ [26], that is the quantum mechanical analog of the classical phase-space density $f(x, p)$, satisfies the restriction $\int f_W^2(x, p) d^3p d^3x \leq (2\pi\hbar)^{-3}$ (see e.g. [27], note that the equality takes place for a pure state only), here the normalization condition $\int f_W(x, p) d^3p d^3x = 1$ is supposed. It evidently excludes utilization of the delta-function as factor in the structure of the Wigner function. Therefore, in order to escape contradiction with quantum mechanics, an another prescription, instead of utilization of delta function, should be used for the longitudinal part of distribution $f(x, p)$; it can be, for example, the boost-invariant prescriptions used in Ref. [17]. Following to this receipt the smearing of δ -function at hypersurface τ_0 in (11) as follows

$$\frac{dN}{d^2p_T d^2x_T d\eta dy} = f\left(\frac{T_{\text{eff}}}{\cosh(\eta - y)}\right). \quad (12)$$

In this way we fix the phase-space density (10). This may correspond to quasi-thermal averaged partonic distribution which can be reached at moment τ_0 due to quantum effects (uncertainly principle), different kind of turbulences and Schwinger-like mechanism of pair

production in the pulse of strong color field. It does not mean that the true thermalization which should be supported by a permanent mechanism of partonic interactions is reached at $\tau_0 \approx 3/\Lambda_s \approx 3 \text{ fm}/c$.

As a result we use the following form of boost-invariant phase-space distribution for gluons at the initial hypersurface τ_0 :

$$f_0 = g^{-2} \frac{a_1(\tau_0 m_T \cosh \theta)^{-1}}{\exp\left(\sqrt{m_{\text{eff}}^2(\mathbf{x}_T) + p_T^2} \cosh \theta / T_{\text{eff}}(\mathbf{x}_T)\right) - 1}, \quad (13)$$

here $\theta = \eta - y$, $\mathbf{x}_T = (X, Y) = (x_T \cos \varphi, x_T \sin \varphi)$ and we consider gluons as massless particles, $m_T = p_T$. Such a distribution depends on the effective mass $m_{\text{eff}}(\mathbf{x}_T) = a_2 \Lambda_s(\mathbf{x}_T)$ and the temperature $T_{\text{eff}}(\mathbf{x}_T) = a_3 \Lambda_s(\mathbf{x}_T)$ (numerical values for a_2 and a_3 are the same as in Eq. (7)), which, in accordance with Ref. [22], are determined by the local scale $\Lambda_s(\mathbf{x}_T)$ (8).

The components of the energy-momentum tensor in the pseudo-Cartesian coordinates reads

$$T^{\mu\nu}(x) = \int p^\mu p^\nu f(x, p) p_T dp_T dy d\phi, \quad (14)$$

where the Lorentz-invariant integration measure d^3p/p_0 in the Cartesian variables is already re-written in Björken variables as $p_T dp_T dy d\phi$.

We numerically calculate the components of the energy-momentum tensor with the distribution function, following from Eq. (13), at $\eta = 0$.

Note that, at $\tau = \tau_0$, the energy-momentum tensor takes the form

$$T_0^{\mu\nu}(\mathbf{x}_T, x_L = 0) = \frac{a_1}{g^2 \tau_0} \Lambda_s^3(\mathbf{x}_T) t^{\mu\nu}, \quad (15)$$

where $t^{\mu\nu}$ are the constant coefficients fixed by the constants a_2 and a_3 . Therefore, the energy profile in transverse plane at τ_0 in central collisions can be presented in the form (see (8))

$$\epsilon(x_T) = \epsilon_0 \frac{\rho^{3/2}(0, x_T)}{\rho_0^{3/2}}, \quad (16)$$

where the number of participants is defined by (3). Under the same reason as for the Glauber-like IC we use the form of this profile to build the IC for hydrokinetic evolution at the thermalization time $\tau_i = 1 \text{ fm}/c$. The maximal energy density ϵ_0 at (proper) time τ_i is the fitting parameter as in the case of the Glauber IC.

III. THE THERMAL MATTER IN A+A COLLISION AND EQUATION OF STATE

Here we describe the matter properties and its thermodynamic characteristics, e.g. equation of state, that are necessary components of the hydrokinetic model. We suppose that soon after thermalization the matter created in A+A collision at RHIC energies is in the quark gluon plasma (QGP) state. Also at time τ_i , there is a peripheral region with relatively small initial energy densities: $\epsilon(r) < 0.5 \text{ GeV}/\text{fm}^3$. This part of the matter ("corona") does not transform into QGP and have no chance to be involved in thermalization process [28]. By itself the corona gives no essential contribution to the hadron spectra [28]. One should consider it separately from the thermal bulk of the matter and should not include in hydrodynamic evolution. Therefore we cut the initial Glauber or CGC-like profiles at $\epsilon(r) \leq 0.5 \text{ GeV}/\text{fm}^3$ when consider IC for hydrodynamic evolution of the system.

During the system evolution the QGP is cooling and finally transforms into hadron phase, most probably, according to the crossover scenario. Such a transformation may occur in the interval of the temperatures 170-190 MeV. At the temperature $T = T_{ch} \approx 165 \text{ MeV}$ the chemical freeze-out happens, as demonstrates an analysis of the particle number ratios [29, 30]. The conception of the chemical freeze-out means that at the temperatures $T \geq T_{ch}$ the bulk of the expanding matter is in the local thermal and chemical equilibrium while at $T < T_{ch}$ the chemical composition becomes in some sense frozen: one can neglect the majority of inelastic reactions except for decays of resonances and recombination processes. The hadronic matter in the later thermodynamic region is not in the chemical equilibrium, moreover, the hadronic medium gradually emits particles being in this zone and, so, loose, in addition, also the local thermal equilibrium. Therefore, one should consider in different ways the matter evolution in the two 4D space-time zones separated by the 3D hypersurface corresponding to the isotherm $T = T_{ch} \approx 165 \text{ MeV}$. Let us describe the thermodynamic properties of matter in both these regions.

A. The EoS in the equilibrated space-time domain.

At high temperatures corresponding to the QGP phase and crossover transition to hadron phase we use a realistic EoS [31] adjusted to the lattice QCD results for zero barionic chemical

potential so that it is matched with an ideal chemically equilibrated multicomponent hadron resonance gas at $T_c = 175$ MeV. To take into account a conservation of the net baryon number, electric charge and strangeness in the QGP phase, one has first to make corrections to thermodynamic quantities for nonzero chemical potentials. As it is proposed in [32], a modification of the EoS can be evaluated by using of the Taylor series expansion in terms of the light and strange quark chemical potentials, or analogously in baryon and strange hadronic chemical potentials:

$$\frac{p(T, \mu_B, \mu_S)}{T^4} = \frac{p(T, 0, 0)}{T^4} + \frac{1}{2} \frac{\chi_B}{T^2} \left(\frac{\mu_B}{T}\right)^2 + \frac{1}{2} \frac{\chi_S}{T^2} \left(\frac{\mu_S}{T}\right)^2 + \frac{\chi_{BS}}{T^2} \frac{\mu_B}{T} \frac{\mu_S}{T} \quad (17)$$

The expansion coefficients χ_B and χ_S are the baryon number and strangeness susceptibilities which are related to thermal fluctuations of baryon number and strangeness in a thermal medium at zero chemical potentials.

To obtain the EoS in the equilibrium zone we use the numerical results for χ_B and χ_S as a function of the temperature given in [32]. The values for the ratios μ_q/T in (17) during the system evolution can be determined approximately. If at some hypersurface corresponding to an isotherm, like as at the chemical freeze-out hypersurface, the chemical potentials are uniform, then the following ratios remain constants

$$\frac{\mu_q}{T} = \text{const}_q, \quad \text{where } q = B, S, E$$

during the chemically equilibrated isentropic evolution of the Boltzmann massless gas. In our approximation we use these constraints and find the corresponding constants from the chemical potentials obtained together with T_{ch} from an analysis of the particle number ratios. In concrete calculations we use the chemical freeze-out temperature $T_{ch} = 165$ MeV, corresponding chemical potentials $\mu_B = 29$ MeV, $\mu_S = 7$ MeV, $\mu_E = -1$ MeV and also the strangeness suppression factor $\gamma_S = 0.935$ which are dictated by 200A GeV RHIC particle number ratios analysis done in the statistical model [29, 30].

B. The EoS in the chemically non-equilibrated domain.

At the chemical freeze-out temperature T_{ch} the "lattice" EoS taken from [31] and corrected for non-zero chemical potentials is matched with good accuracy with ideal Boltzmann hadronic resonance gas which includes $N = 359$ hadron states made of u, d, s quarks with

masses up to 2.6 GeV. Essentially, we use the same particle set in the FASTMC event generator [33]. Technically, in the numerical code, we input the corresponding N functions - the densities n_i of each hadron i and the equations for n_i already at the very beginning of the system evolution; however, these densities are meaningless in the QGP phase and their evaluation does not influence on the system evolution in the equilibrated zone. These functions are brought into play at $T < T_{ch}$. If this thermodynamic region would correspond to the complete conservation of the particle numbers then, in addition to the energy-momentum conservation, one would account for the conservation equations for particle number flows in the form:

$$\partial_\mu(n_i u^\mu) = 0, \quad i = 1 \dots N \quad (18)$$

In our problem, however, during the system evolution in the non-equilibrated zone $T < T_{ch}$ the resonance decays have to be taken into account. The decay law in a homogeneous medium with $T \ll m_i$ (m_i is the resonances mass) implies a summing up of a decrease of unstable i th particle number due to decays and an increase because of decays of heavier j th resonance into i th particle:

$$\frac{dN_i}{dt} = -\Gamma_i N_i + \sum_j b_{ij} \Gamma_j N_j \quad (19)$$

where Γ_i is the total width of resonance i , $b_{ij} = B_{ij} M_{ij}$ denote the average number of i th particles coming from arbitrary decay of j th resonance, $B_{ij} = \Gamma_{ij}/\Gamma_{j,tot}$ is branching ratio, M_{ij} is a number of i th particles produced in $j \rightarrow i$ decay channel. The set on N equations (19), solved together, takes into account all possible cascade decays $i \rightarrow j \rightarrow k \rightarrow \dots$. This also conserves net charges, e.g. baryon, electric charge and strangeness, since the charges are conserved in resonance decay process. If one relates the Eq. (19) to the fluid element of some volume ΔV moving with four-velocity u^μ , then a covariant relativistic extension of the decay law for a hydrodynamic medium leads to the equation (18):

$$\partial_\mu(n_i(x)u^\mu(x)) = -\Gamma_i n_i(x) + \sum_j b_{ij} \Gamma_j n_j(x) \quad (20)$$

when one neglects a thermal motion of the resonance j , that can be justified because post (chemical) freeze-out temperatures are much less than the mass of the lightest known resonance. Also, Eq. (20) for the hydrodynamic evolution is written under supposition of an instant thermalization of the decay products, that is consistent with the ideal fluid approximation (mean free path is zero). In the kinetic part of the HKM we consider the next

approximation when the non-equilibrium character of the distribution functions and the kinetics of resonance decays are taken into account. We also can approximately account for a recombination in the processes of resonance decays into expanding medium just by utilizing the effective decay width $\Gamma_{i,eff} = \gamma\Gamma_i$ in Eq. (20). We use $\gamma = 0.75$ [34] for the resonances containing u and d quarks supposing thus that about 30% of such resonances are recombining during the evolution.

The equations (20) together with the hydrodynamic equations and the equation of state should give one the energy density and composition of the gas in each space-time points. To find the EoS $p = p(\epsilon, \{n_i\})$ for the mixture of hadron gases we start with the expressions for energy density and particle density for i th component of multicomponent Boltzmann gas :

$$\begin{aligned}\epsilon_i &= \frac{g_i}{2\pi^2} m_i^2 T (3TK_2(m_i/T) + m_i K_1(m_i/T)) \exp(\mu_i/T) \\ n_i &= \frac{g_i}{2\pi^2} m_i^2 T K_2(m_i/T) \exp(\mu_i/T).\end{aligned}\tag{21}$$

Then, the equation for the temperature is:

$$\epsilon = 3nT + \sum_i n_i m_i \frac{K_1(m_i/T)}{K_2(m_i/T)},\tag{22}$$

where $n = \sum_i n_i$. Having solved this equation numerically for given ϵ and $\{n_i\}$, we get the temperature and then find the pressure using simple relation for multicomponent Boltzmann gas:

$$p = nT\tag{23}$$

The equations (22), (23) define $p = p(\epsilon, \{n_i\})$.

Thus, we follow the evolution of all N densities of hadron species in hydro calculation, and compute EoS dynamically for each chemical composition of N sorts of hadrons in every hydrodynamic cell in the system during the evolution. Using this method, we do not limit ourselves in chemically frozen or equilibrated evolution, keeping nevertheless thermodynamically consistent scheme.

As it was mentioned before, we use the Boltzmann approximation in the EoS calculation to decrease computational time. However, for emission function and spectra calculation we use quantum Bose-Einstein/Fermi-Dirac distribution functions with chemical potentials calculated to give the same particle densities as in the Boltzmann case. We checked that the measure of relative divergence in the energy density if one uses the quantum distribution

functions instead of the Boltzmann one, is not bigger than 3% in the thermodynamic region which is actually contributed to formation of hadronic spectra.

IV. KINETICS IN THE NON-EQUILIBRIUM HADRONIC ZONE

To describe the non-equilibrium evolution and decay of hadronic system we start from the Boltzmann equations for the mixture of hadrons, most of which have finite lifetimes and decay widths compatible with particle masses. The set of such equations for i -components of the hadron resonance gas which account for the only binary interactions (elastic scattering) and resonance decays are:

$$\frac{p_i^\mu}{p_i^0} \frac{\partial f_i(x, p)}{\partial x^\mu} = G_i^{scatt} - L_i^{scatt}(x, p) + G_i^{decay}(x, p) - L_i^{decay}(x, p) \equiv G_i(x, p) - L_i(x, p). \quad (24)$$

Here we ignore the processes of resonance recombination which simpler to account phenomenologically (see the previous Section). The term gain (G) describes an income of the particles into phase-space point (x, p) due to scatters and resonance decays. The term *loss* (L) is related to a decrease of particles in the vicinity of the phase space point (x, p) due to re-scattering and decays of resonances. The *loss* term is proportional to the particle number density in the point x and so $L_i^{scatt}(x, p) = f_i R_i$, $L_i^{decay}(x, p) = f_i D_i$ where R is scattering rate, and D is decay rate. If one considers the equations for stable or quasi-stable particles, then $L_i^{decay}(x, p) = 0$ ($D_i \equiv 0$).

The method allowing to find the emission function of the hadrons based on the Boltzmann equations in the (generalized) relaxation time approximation was proposed in Refs. [5, 6]. Following to this method we put: $J_i(x, p) \approx R_{i,l.eq.}(x, p)$, $G_i \approx R_{i,l.eq.}(x, p) f_{i,l.eq.}(x, p) + G_i^{decay}(x, p)$. The quantity $R(x, p) = \tau_{rel}^{-1}(x, p)$ is the inverse relaxation time, or collision rates in global reference frame. Then,

$$\frac{p^\mu}{p^0} \partial_\mu f_i(x, p) = (f_i^{l.eq.}(x, p) - f_i(x, p)) R_i(x, p) + G_i^{decay}(x, p) - L_i^{decay}(x, p) \quad (25)$$

The explicit form of $G_i^{decay}(x, p)$ term will be derived later. In the first approximation to hydro-kinetic evolution the parameters of the local equilibrium distribution function $f_{i,l.eq.}(x, p)$, e.g. the temperature $T(x)$, chemical potentials $\mu_i(x)$ are determined by the hydrodynamic evolution. The details of hydrodynamic approach used in the model are described in the next section.

A. Emission functions in hyperbolic coordinates and spectra formation

All our results are related to the very central rapidity interval, $y \approx 0$, and we will use the boost-invariant approach to describe strong longitudinal matter expansion observed at RHIC. For such an approach the hyperbolic coordinates in (t, x_L) directions are more suitable than the Cartesian ones. Then the kinetic equations take a form

$$\frac{1}{m_T \cosh y} \left(m_T \cosh \theta \frac{\partial}{\partial \tau} - \frac{m_T \sinh \theta}{\tau} \frac{\partial}{\partial \eta} + \vec{p}_T \frac{\partial}{\partial \vec{r}_T} \right) f_i(\tau, \theta, \mathbf{r}_T, \mathbf{p}_T) = \left[f_i^{l.eq.}(\tau, \theta, \mathbf{r}_T, \mathbf{p}_T) - f_i(\tau, \theta, \mathbf{r}_T, \mathbf{p}_T) \right] R_i(\tau, \theta, \mathbf{r}_T, \mathbf{p}_T) + G_i^{decay}(\tau, \theta, \mathbf{r}_T, \mathbf{p}_T) \quad (26)$$

where $\tau = \sqrt{t^2 - x_L^2}$ is a proper time, $m_T = \sqrt{m^2 + p_T^2}$ is a transverse mass, $\theta = \eta - y$, η is a space-time rapidity, defined above Eq. (7), and y is a particle rapidity.

The formal solutions of (26) correspond to the non-equilibrium distribution functions in expanding and decaying multi-hadronic system:

$$f_i(\tau, \theta, \mathbf{r}_T, \mathbf{p}_T) = f_i^{l.eq.}(\tau_0, \theta^{(\tau_0)}(\tau), \mathbf{r}_T^{(\tau_0)}(\tau), \mathbf{p}_T) \exp \left(- \int_{\tau_0}^{\tau} \tilde{R}_i(s, \theta^{(s)}(\tau), \mathbf{r}_T^{(s)}(\tau), \mathbf{p}_T) ds \right) + \int_{\tau_0}^{\tau} d\lambda \left[f_i^{l.eq.}(\lambda, \theta^{(\lambda)}(\tau), \mathbf{r}_T^{(\lambda)}(\tau), \mathbf{p}_T) \tilde{R}_i(\lambda, \theta^{(\lambda)}(\tau), \mathbf{r}_T^{(\lambda)}(\tau), \mathbf{p}_T) + \tilde{G}_i^{decay}(\lambda, \theta^{(\lambda)}(\tau), \mathbf{r}_T^{(\lambda)}(\tau), \mathbf{p}_T) \right] \quad (27)$$

$$\exp \left(- \int_{\lambda}^{\tau} \tilde{R}_i(s, \theta^{(s)}(\tau), \mathbf{r}_T^{(s)}(\tau), \mathbf{p}_T) ds \right)$$

here $\tilde{R}_i(\lambda, \theta, \mathbf{r}_T, \mathbf{p}_T) = \frac{\cosh y}{\cosh \theta} R_i(\lambda, \theta, \mathbf{r}_T, \mathbf{p}_T)$, $\tilde{G}_i^{decay}(\lambda, \theta, \mathbf{r}_T, \mathbf{p}_T) = \frac{\cosh y}{\cosh \theta} G_i^{decay}(\lambda, \theta, \mathbf{r}_T, \mathbf{p}_T)$.

Here we use the notation

$$\begin{cases} \sinh \theta^{(\tau_0)}(\tau) = \frac{\tau}{\tau_0} \sinh \theta \\ \mathbf{r}_T^{(\tau_0)}(\tau) = \mathbf{r}_T - \frac{\mathbf{p}_T}{m_T} (\tau \cosh \theta - \sqrt{\tau_0^2 + \tau^2 \sinh^2 \theta}) \end{cases} \quad (28)$$

The invariant value is $p^0 R_i(x, p) = p^{*0} R_i^*(x, p)$, where the asterisk * denotes a value in the local rest frame of the fluid element in point x , so

$$\tilde{R}_i(x, p) = \frac{\cosh y}{\cosh \theta} R_i(x, p) = \frac{\cosh y}{\cosh \theta} \frac{p^\mu u_\mu}{p^0} R_i^*(p, T) = \frac{p^\mu u_\mu}{m_T \cosh \theta} R_i^*(p, T) \quad (29)$$

To connect the formal solution (27) with observables, e.g. particle spectrum, we use the equality

$$p^0 \frac{d^3 n}{d^3 p} = \frac{d^2 n}{2\pi p_T dp_T dy} = \int_{\sigma_{out}} d\sigma_\mu p^\mu f(x, p) \quad (30)$$

where σ_{out} is a "distant" hypersurface of large $\tau = const$, where all the interactions among hadrons are ceased.

In what follows we use the variable substitution in the first term of (27) describing the "initial emission" :

$$\begin{cases} \sinh \theta = \frac{\tau_0}{\tau} \sinh \theta' \\ \mathbf{r}_T = \mathbf{r}'_T + \frac{\mathbf{p}_T}{m_T} (\tau \cosh \theta - \sqrt{\tau_0^2 + \tau^2 \sinh^2 \theta}) \end{cases} \quad (31)$$

and the substitution :

$$\begin{cases} \sinh \theta = \frac{\lambda}{\tau} \sinh \theta' \\ \mathbf{r}_T = \mathbf{r}'_T + \frac{\mathbf{p}_T}{m_T} (\tau \cosh \theta - \sqrt{\lambda^2 + \tau^2 \sinh^2 \theta}) \end{cases} \quad (32)$$

in the second term of (27) related to the "4-volume emission". After transformation to new variables $\{\tau, \theta', \vec{r}'\}$ we arrive with the result:

$$\begin{aligned} \int_{\sigma_{out}} d\sigma_\mu p^\mu f(x, p) &= \int_{\sigma_0} d\sigma_0^\mu p_\mu f_i^{l.eq.}(\tau_0, \theta', \mathbf{r}'_T, p) \exp \left(- \int_{\tau_0}^{\infty} \tilde{R}_i(s, \theta^{(s)}(\tau_0), \mathbf{r}'_T^{(s)}(\tau_0), \mathbf{p}_T) ds \right) + \\ &\int_{\tau_0}^{\tau} d\lambda \int_{\sigma(\lambda)} d\sigma_\mu(\lambda) p^\mu \left[f_i^{l.eq.}(\lambda, \theta', \mathbf{r}'_T, \mathbf{p}_T) \tilde{R}_i(\lambda, \theta', \mathbf{r}'_T, \mathbf{p}_T) + \tilde{G}_i^{decay}(\lambda, \theta', \mathbf{r}'_T, \mathbf{p}_T) \right] \cdot \\ &\cdot \exp \left(- \int_{\lambda}^{\infty} \tilde{R}_i(s, \theta^{(s)}(\lambda), \mathbf{r}'_T^{(s)}(\lambda), \mathbf{p}_T) ds \right) = p^0 \frac{d^3 N}{d^3 p} \end{aligned} \quad (33)$$

where $\sigma(\lambda)$ is $\tau = \lambda = const$ hypersurface, so $d\sigma_\mu(\lambda) p^\mu = \lambda m_T \cosh \theta' d\theta' d^2 \vec{r}'_T$. The exponential values in these expressions are the escape probabilities

$$\mathcal{P}(\tau, \mathbf{r}_T, \theta, \mathbf{p}_T) = \exp \left(- \int_{\tau}^{\infty} \tilde{R}_i(s, \theta^{(s)}(\tau), r_T^{(s)}(\tau), \mathbf{p}_T) ds \right) \quad (34)$$

for particles with momentum p at space-time point $(\tau, \mathbf{r}_T, \eta = \theta + y)$ (in hyperbolic coordinates) to become free without any collision [5, 6].

In the expression above we can separate the 4-volume emission function

$$S_i(\lambda, \theta, \mathbf{r}_T, \mathbf{p}_T) = \left[f_i^{l.eq.}(\lambda, \theta, \mathbf{r}_T, p) \tilde{R}_i(\lambda, \theta, r_T, p) + \tilde{G}_i^{decay}(\lambda, \theta, \mathbf{r}_T, \mathbf{p}_T) \right] \mathcal{P}(\lambda, \mathbf{r}_T, \theta, \mathbf{p}_T) \quad (35)$$

and the initial emission :

$$S_{i,0}(\theta, \mathbf{r}_T, \mathbf{p}_T) = f_i^{l.eq.}(\tau_0, \theta, \mathbf{r}_T, \mathbf{p}_T) \mathcal{P}(\tau_0, \mathbf{r}_T, \theta, \mathbf{p}_T) \quad (36)$$

These expressions demonstrate obviously that the particle emission is formed by the particles which undergo their *last* interaction or are already free initially. These expressions for the hadron emission function are the basic functions for calculations of the single- and multi-particle spectra [5]. To evaluate these quantities for observed (quasi) stable particles one needs to find the term gain G_i^{decay} for resonance decays and the collision rates R_i .

B. Resonance decays in multi-component gas

We suppose that in the first (hydrodynamic) approximation the products of resonance decays which interact with medium are thermalized and they become free later, after the last collision with one of other particles. However, at the late stages of matter evolution the system becomes fairly dilute, so that some of these produced particles get a possibility to escape without any collisions: $\mathcal{P} > 0$. To describe this we use the following form for L_i^{decay} and G_i^{decay} terms (for 2-particle resonance decay) [35]:

$$p_i^0 L_i^{decay}(x, p_i) = \sum_k \sum_l \int \frac{d^3 p_k}{p_k^0} \int \frac{d^3 p_l}{p_l^0} \Gamma_{i \rightarrow kl} f_i(x, p_i) \frac{m_i}{F_{i \rightarrow kl}} \delta^{(4)}(p_i - p_k - p_l) = m_i \Gamma_i f_i(x, p_i) \quad (37)$$

where resonance i decays into particles or resonances k and l .

$$p_i^0 G_i^{decay}(x, p_i) = \sum_j \sum_k \int \frac{d^3 p_j}{p_j^0} \int \frac{d^3 p_k}{p_k^0} \Gamma_{j \rightarrow ik} f_j(x, p_j) \frac{m_j}{F_{j \rightarrow ik}} \delta^{(4)}(p_j - p_k - p_i) \quad (38)$$

where the resonance j decays into particles i and k with partial width $\Gamma_{j \rightarrow ik}$ for this decay channel, and

$$F_{j \rightarrow ik} = \int \frac{d^3 p_k}{p_k^0} \int \frac{d^3 p_i}{p_i^0} \delta^{(4)}(p_j - p_k - p_i) = \frac{2\pi}{m_j^2} ((m_j^2 - m_k^2 - m_i^2)^2 - 4m_i^2 m_k^2)^{1/2} \quad (39)$$

To escape the complicated problem with satisfaction of thermodynamic identities in hadron resonance gas we utilize in what follows the mass shell approximation for resonances, supposing that $m_i = \langle m_i \rangle$. Also, as it was already discussed, we take into account that the resonance mass in hadron resonance gas is much larger than the temperature, $m_i \gg T_c$. Then the most probable velocity of resonance in the rest system of a fluid element is small, $\bar{v}_i \approx \sqrt{\frac{2T}{m_i}}$, and one can use the approximation

$$p_i^\mu \approx m_i u^\mu. \quad (40)$$

So the resonance distribution function takes the form

$$f_j(x, p_i) \approx \frac{p_j^0}{m_j} n_j(x) \delta^3(\mathbf{p}_j - m_j \mathbf{u}(x)), \quad (41)$$

It allows us to perform integrations in (38) over p_j, p_k analytically and get :

$$G_i^{decay}(x, p_i) = \sum_j \sum_k \Gamma_{j \rightarrow ik} \frac{n_j(x)}{p_i^0 p_k^0 F_{j \rightarrow ik}} \delta(m_j u^0(x) - p_k^0 - p_i^0) \quad (42)$$

where $p_k^0 = \sqrt{m_k^2 + (m_j \mathbf{u}(x) - \mathbf{p}_i)^2}$.

Just this form of gain term is used when spectra are evaluated according to Eq. (33). Note that in practical calculations we substitute δ -function by its Gaussian representation:

$$\delta(x) = \frac{1}{R\sqrt{\pi}} e^{-x^2/R^2}$$

and take a finite parameter value $R = 50 MeV$.

C. Collision rates

The collision rate $R(x, p) = \frac{1}{\tau_{rel}(x, p)}$ is one of the basic value for calculation of the intensity of the interactions in the expanding system and its decoupling. The latter is described through the escape probability $\mathcal{P}(x, p)$ (34) - the integral value of R along the possible trajectory of a particle with momentum p running freely through the whole expanding system. The rate of collisions in the rest frame of some fluid element that accounts for scatters of given particle with any other i th hadronic species in the thermal Boltzmann system depends only on particle energy $E_p^* = p^\mu u_\mu$ and the thermodynamic parameters of this fluid element [36]:

$$R^*(E_p^*, T, \{\mu_i\}) = \sum_i \int d^3 k_i \frac{g_i}{(2\pi)^3} \exp\left(-\frac{E_{k,i} - \mu_i(x)}{T(x)}\right) \sigma_i(s_i) \frac{\sqrt{(s_i - (m - m_i)^2)(s_i - (m + m_i)^2)}}{2E_p^* E_{k,i}} \quad (43)$$

Here $g_i = (2j_i + 1)$, $E_p = \sqrt{\mathbf{p}^{*2} + m^2}$, $E_{k,i} = \sqrt{\mathbf{k}_i^2 + m_i^2}$, $s_i = (p^* + k_i)^2$ is the squared c.m. energy of the pair, and $\sigma_i(s)$ is the total cross section of selected particle with particle i in the corresponding binary collision. One can change the integration variable to squared center of mass energy s , energy of scattering partner E_k and momentum angle ϕ , and perform E_k

and ϕ -integration analytically, which gives the expression for remaining integral:

$$R^*(E_p^*, T, \{\mu_i\}) = \sum_i \frac{g_i T e^{\mu_i/T}}{8\pi^2 p^* E_p^*} \int_{(m+m_i)^2}^{\infty} ds \sigma_i(s) \sqrt{(s - m^2 - m_i^2)^2 - 4m_i^2 m^2} \times \\ \times \sinh\left(\frac{p^*}{2Tm^2} \sqrt{(s - m^2 - m_i^2)^2 - 4m_i^2 m^2}\right) \exp\left(-\frac{(s - m^2 - m_i^2)E_p^*}{2Tm^2}\right) \quad (44)$$

We calculate $\sigma_i(s)$ in a way similar to UrQMD code [37]:

- Breit-Wigner formula is applied for meson-meson and meson-baryon scattering:

$$\sigma_{total}^{MB}(\sqrt{s}) = \sum_{R=\Delta, N^*} \langle j_B, m_B, j_M, m_M || J_R, M_R \rangle \frac{2S_R + 1}{(2S_B + 1)(2S_M + 1)} \\ \times \frac{\pi}{p_{cm}^2} \frac{\Gamma_{R \rightarrow MB} \Gamma_{total}}{(M_R - \sqrt{s})^2 + \Gamma_{tot}^2/4} \quad ,$$

where $\Gamma_{total} = \sum_{(\text{channels})} \Gamma_{R \rightarrow MB}$, with \sqrt{s} -dependent parametrization of partial decay widths:

$$\Gamma_{R \rightarrow MB}(M) = \Gamma_R \frac{M_R}{M} \left(\frac{p_{CMS}(M)}{p_{CMS}(M_R)} \right)^{2l+1} \frac{1.2}{1 + 0.2 \left(\frac{p_{CMS}(M)}{p_{CMS}(M_R)} \right)^{2l}}$$

chosen to depend on absolute value of particle momentum in two-particle rest frame:

$$p_{CMS}(\sqrt{s}) = \frac{1}{2\sqrt{s}} \sqrt{(s - m_1^2 - m_2^2)^2 - 4m_1^2 m_2^2}$$

In the case of meson-meson scattering a constant elastic cross section of 5 mb is added in order to fully reproduce the measured cross section.

- PDG table data for $p - p$, $p - n$, $p - \bar{p}$, etc. scattering
- other baryon-baryon scattering: additive quark model:

$$\sigma_{total} = 40 \left(\frac{2}{3} \right)^{m_1+m_2} \left(1 - 0.4 \frac{s_1}{3 - m_1} \right) \left(1 - 0.4 \frac{s_2}{3 - m_2} \right) [\text{mb}] \quad ,$$

$m_i = 1(0)$ corresponds to meson(baryon), s_i - number of strange quarks in hadron i .

Note that all relevant resonance states (see above), 359 different species - are taken into account for the calculation of $\sigma_i(s)$.

V. HYDRODYNAMICS

We describe the system evolution in the equilibrium zone at $T > T_{ch}$ by the perfect hydrodynamics. The small shear viscosity effects, which lead to an increase of the transverse flows [10] we account phenomenologically including this effect in the parameter α of initial velocity as described in Section IIA. The matter evolution in this zone is described by the relativistic hydrodynamical equations related to the conservation of energy-momentum:

$$\partial_\nu T^{\mu\nu} = 0 \quad (45)$$

and equations associated with the net baryon number, strangeness and isospin conservations

$$\partial_\nu (q_i u^\nu) = 0 \quad (46)$$

Here q_i is the density of conserved quantum number.

At $T < T_{ch}$ the equations for the system evolution in the first approximation: $f_i = f_i^{l.eq}$ can be derived from the basic equation (25). Namely, integrating the left and right hand sides of Eq.(25) over d^3p one arrives to the equation (20) for particle number flow in the non-equilibrium zone, and also to hydrodynamic equation (45) by integrating Eq. (25) over $p_i^\nu d^3p_i$ and summing over index i .

Note that in the first approximation the matter evolution is described by the equations of ideal hydrodynamics while the distribution function (27) in decaying system is non-equilibrium. The iteration procedure, including the next order approximations, that, in fact, leads to viscous hydrodynamic evolution, is described in Ref. [6]. In this article we limit ourself by the first approximation. Then the energy-momentum tensor $T^{\mu\nu}$ has a simple structure which is employed in this model :

$$T^{\mu\nu} = (\epsilon + p)u^\mu u^\nu - p \cdot g^{\mu\nu}, \quad (47)$$

where ϵ is energy density and p is pressure defined from the EoS. In the chemically equilibrated zone the pressure is defined from the lattice QCD calculations as discussed in Section IIIA. In the non-equilibrium zone the EoS generally depends on all 360 variables, $p = p(\epsilon, \{n_i\})$, and it is evaluated altogether with solution of the evolutionary equations. The reason is that it is impossible to store the EoS table, therefore we compute pressure each time we need it (e.g. when restoring thermodynamic variables from conservative variables

or when computing fluxes through each cell boundary) solving analytic equations (22), (23) numerically.

Let us rewrite equations in hyperbolic coordinates. These coordinates are suitable for dynamical description at RHIC energies, since, for example, zero longitudinal flows correspond to boost-invariant expansion (so nonzero longitudinal flow correspond to deviation from boost invariance), and evolution parameter, $\tau = \sqrt{t^2 - x^2}$ is not affected by strong longitudinal flow, which saves computational time. It is convenient to write the equations in conservative form, then the conservative variables are :

$$\vec{Q} = \begin{pmatrix} Q_\tau \\ Q_x \\ Q_y \\ Q_\eta \\ \{Q_{n_i}\} \end{pmatrix} = \begin{pmatrix} \gamma^2(\epsilon + p) - p \\ \gamma^2(\epsilon + p)v_x \\ \gamma^2(\epsilon + p)v_y \\ \gamma^2(\epsilon + p)v_\eta \\ \{\gamma n_i\} \end{pmatrix}. \quad (48)$$

Here the expression in curly brackets denote N variables associated with the particle densities for each sort of hadrons. The Q_i are conservative variables in the sense that integral (discrete sum over all cells) of Q_i gives the total energy, momentum and particle numbers, which are conserved up to the fluxes on the grid boundaries. The velocities in this expression are defined in LCMS (longitudinally co-moving system), and related to velocities in the laboratory frame as :

$$\begin{aligned} v_x &= v_x^{lab} \cdot \frac{\cosh y_f}{\cosh(y_f - \eta)} \\ v_y &= v_y^{lab} \cdot \frac{\cosh y_f}{\cosh(y_f - \eta)} \\ v_\eta &= (y_f - \eta), \end{aligned} \quad (49)$$

where $y_f = \frac{1}{2} \ln[(1 + v_z^{lab})/(1 - v_z^{lab})]$ is the longitudinal rapidity of fluid element, $\eta = \frac{1}{2} \ln[(t + z)/(t - z)]$ is the geometrical rapidity.

The full hydrodynamical equations are :

$$\partial_\tau \underbrace{\begin{pmatrix} Q_\tau \\ Q_x \\ Q_y \\ Q_\eta \\ \{Q_{n_i}\} \end{pmatrix}}_{\text{quantities}} + \vec{\nabla} \cdot \underbrace{\begin{pmatrix} Q_\tau \\ Q_x \\ Q_y \\ Q_\eta \\ \{Q_{n_i}\} \end{pmatrix}}_{\text{fluxes}} \vec{v} + \underbrace{\begin{pmatrix} \vec{\nabla}(p \cdot \vec{v}) \\ \partial_x p \\ \partial_y p \\ \frac{1}{\tau} \partial_\eta p \\ 0 \end{pmatrix}}_{\text{fluxes}} + \underbrace{\begin{pmatrix} (Q_\tau + p)(1 + v_\eta^2)/\tau \\ Q_x/\tau \\ Q_y/\tau \\ 2Q_\eta/\tau \\ \{Q_{n_i}/\tau\} \end{pmatrix}}_{\text{sources}} = 0 \quad (50)$$

and $\vec{\nabla} = (\partial_x, \partial_y, \frac{1}{\tau} \partial_\eta)$.

For hydrodynamic calculations related to midrapidity region on central A+A collisions we impose longitudinal symmetry and cylindrical symmetry in transverse direction. This actually means that tangential (in transverse direction) and longitudinal velocities in LCMS vanish, so $Q_\phi = Q_\eta = 0$, as well as the fluxes in ϕ and η directions. Then, one has to solve the following set of equations :

$$\partial_\tau \underbrace{\begin{pmatrix} Q_\tau \\ Q_r \\ \{Q_{n_i}\} \end{pmatrix}}_{\text{quantities}} + \partial_r \cdot \underbrace{\begin{pmatrix} (Q_\tau + p)v_r \\ Q_r v_r + p \\ \{Q_{n_i} v_r\} \end{pmatrix}}_{\text{fluxes}} + \underbrace{\begin{pmatrix} (Q_\tau + p)(1 + v_\eta^2)/\tau - (Q_\tau + p)v_r/r \\ Q_r/\tau - Q_r v_r/r \\ \{Q_{n_i}/\tau - Q_{n_i} v_r/r\} \end{pmatrix}}_{\text{sources}} = 0 \quad (51)$$

Practically v_r/r is ambiguous at $r = 0$, so we put $v_r/r = \alpha$ there and use α value interpolated from the neighboring points.

We base our calculations on the finite-volume approach: we discretize the system on a fixed grid in the calculational frame and interpret Q_i^n as average value over some space interval i , which is called a cell (i is a multi-index in multidimensional case). We also split continuous time evolution into a sequence of finite timesteps n .

The Q_i^n are then updated after each timestep according to the fluxes on the cell interface during the timestep Δt_n . In 3-dimensional case one has the following update formula :

$$Q_{ijk}^{n+1} = Q_{ijk}^n - \frac{\Delta t}{\Delta x_1} (F_{i+1/2,jk} + F_{i-1/2,jk}) - \frac{\Delta t}{\Delta x_2} (F_{i,j+1/2,k} + F_{i,j-1/2,k}) - \frac{\Delta t}{\Delta x_3} (F_{ij,k+1/2} + F_{ij,k-1/2}) \quad (52)$$

Where F is the average flux over the cell boundary, indexes $+1/2$ and $-1/2$ correspond to right and left cell boundary in each direction.

This is a base of the Godunov method [39] that implies that the distributions of variables on the grid are piecewise, this forms the Riemann problem at each cell interface. Then the

flux through each cell interface depends only on the solution of single Riemann problem, supposing that the waves from the neighbouring discontinuities do not intersect. The latter is satisfied with Courant-Friedrichs-Lewy (CFL) condition [40].

To solve the Riemann problems at each cell interface we use relativistic HLLC solver [38], which approximates the wave profile in the Riemann problem by single intermediate state between two shock waves propagating away from the initial discontinuity. Together with the shock wave velocity estimate, in this approximation one can obtain analytical dependence of flux on initial conditions for Riemann problem, which makes algorithm to be explicit.

We proceed then to construct higher-order numerical scheme. To do so,

- in time : the *predictor-corrector* scheme is used for the second order of accuracy in time, i.e. the numerical error is $O(dt^3)$, instead of $O(dt^2)$
- in space : in the same way, to achieve the second order scheme the *linear distributions* of quantities (conservative variables) inside cells are used.

— *Multi-dimension problem.* At each timestep, we compute and sum the fluxes for each cell with all its neighbours and update the value of conservative variables with the total flux. Thus, we do not use operator splitting (dimensional splitting) and thus avoid the numerical artifacts introduced by this method, e.g. artificial spatial asymmetry.

— *Grid boundaries.* To treat grid boundaries, we use the method of *ghost cells*. We include the two additional cells on either end of grid in each direction, and set the quantities in these cells at the beginning of each timestep. For simplicity, we set the quantities in ghost cells to be equal to these in the nearest "real" cell, thus implementing nonreflecting boundary conditions (outflow boundary). This physically correspond to boundary which does not reflect any wave, which is consistent with expansion into vacuum.

— *Vacuum treatment.* In our simulations we deal with spatially finite systems expanding into vacuum. Thus computational grid in the Eulerian algorithm must initially contain both system and surrounding vacuum. To account for a finite velocity of expansion into vacuum, which equals c for infinitesimal slice of matter on the boundary, we introduce additional (floating-point) variables in each cell which keep the extent of matter expansion within a cell, having value 1 for the complete cell, 0 for a cell with vacuum only. The matter is allowed to expand in the next vacuum cell only if the current cell is filled with the matter.

VI. RESULTS AND DISCUSSION

In the article we apply the hydrokinetic model for an analysis of the space-time picture of Au+Au collisions at the top RHIC energies. Such an analysis provided in the evolutionary models of heavy ion collisions have to be based on a detailed description of the pion and kaon femtoscopic scales and must also describe well the *absolute* values of the spectra (not only spectra slopes) of the particles. As it was noted in Ref. [6], the following factors favor the simultaneous description of the mentioned data: a relatively hard EoS (crossover transition between hadronic and quark-gluon matters, not the first order phase transition), the pre-thermal transverse flows developed to thermalization time, an account for an "additional portion" of the transverse flows due to the shear viscosity effect [10], a correct description of the gradual decay of the system at the late stage of the expansion. All these factors are included in the presented version of the HKM.

We use both the Glauber-like (Section IIB) and CGC-like (Section IIC) initial conditions. In the former case the mean transverse radii, defined by (1) is $R_T = 4.137$ fm for the top RHIC energy. The best fit for the Glauber IC is reached at the following values of the two fitting parameters related to the proper time $\tau = 1$ fm/c: $\epsilon_0 = 16.5$ GeV/fm³ ($\langle\epsilon\rangle = 11.69$ GeV/fm³) and parameter of the initial velocity defined by (1), $\alpha = 0.248$ ($\langle v_T \rangle = 0.224$). In the case of the CGC-like initial conditions $R_T = 3.88$ fm, the fitting parameters leading to the best data description are $\epsilon_0 = 19.5$ GeV/fm³ ($\langle\epsilon\rangle = 13.22$ GeV/fm³) and $\alpha = 0.23$ ($\langle v_T \rangle = 0.208$). The parameters α for the initial transverse flows are somewhat larger than they are for the free streaming approximation of the pre-thermal stage [17]. The reason is, as it is explained in Section II, that the fitting parameter α is related to the "unknown portions" of flows, caused by the two factors: a developing of the pre-thermal flows and the viscosity effects in the quark-gluon plasma. In addition, an account of the event-by-event fluctuations of the initial conditions also leads to an increase of the "effective" transverse flows, obtained by averaging at the final stage, as compare to the results based on the initial conditions averaged over initial fluctuations [41]. Since we use the later kind of IC, it should lead also to an increase of the effective parameter α .

As it was discussed in Sections III, the chemically non-equilibrated evolution at the late stage, $T < T_{ch} = 165$ MeV, is not characterized by a simple EoS, like $p = p(\epsilon, \mu_B)$, in our calculations the pressure in this domain depends on 360 variables: energy density and

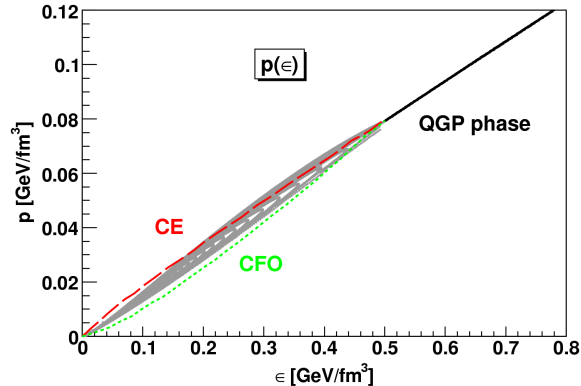


FIG. 1: (Color online) Equation of state $p(\epsilon)$ used in the HKM calculations. The solid black line is related to the chemically equilibrated phase, taken from lattice QCD results as described in Sec. IIIA, while grey region consists of set of the points corresponding to the different hadron gas compositions at each ϵ occurring during the late non-equilibrium stage of the evolution. The dashed line denotes EoS for the chemically equilibrated hadron gas and dotted line for the chemically frozen one, they are shown for a comparison.

particle concentrations. In Fig. 1 we demonstrate the "effective" EoS at the temperatures around and below T_{ch} . The points related to the later region characterize all diapason which the pressure gains at each energy density when the system evolves with the Glauber IC fixed above. We see that the pressure is differ from the "limited" cases: the chemically equilibrated and completely chemically frozen evolution (when the numbers of *all* (quasi) stable particles and resonances are conserved). At relatively large energy densities in a dominated space-time region the non-equilibrium EoS is harder than even in the chemically equilibrated case. This could reduce the out- to side- ratio for transverse interferometry radii.

The results of the HKM for the pion and kaon spectra, interferometry radii and R_{out}/R_{side} ratio are presented in Fig. 2. Since the temperature and baryonic chemical potential at chemical freeze-out, which are taken from the analysis of the particle number ratios [29], are more suitable for the STAR experiment, the HKM results for kaon spectra are good for the STAR data but not so much for the PHENIX ones. Note also that, in spite of other studies (e.g., [4]), we compare our results for the interferometry radii within the whole measured interval of p_T covered at the top RHIC energy. Finally, one can conclude from Fig. 2 that the description of pion and kaon spectra and space-time scales is quite good for both IC,

the Glauber and CGC. It is worth noting, however, that the two fitting parameters α and ϵ_0 are various by 10-20% for different IC, as it is described above.

The special attention acquires a good description of the pion and kaon longitudinal radii altogether with R_{out}/R_{side} ratio, practically, within the experimental errors. Such an achievement means that the HKM catches the main features of the matter evolution in A+A collisions and correctly reproduces the homogeneity lengths in the different parts of the system which are directly related to the interferometry radii at the different momenta of the pairs [2]. In this connection it is valuable to show the structure of the emission function for pions and kaons.

In Fig. 3 we demonstrate the space-time structure of the particle emission at the Glauber IC for different transverse momenta of particles, longitudinal momenta is close to zero. The space-time picture of particle liberation is quite different for different transverse momenta: for the soft particles the maximal emission occurs close to the central part and happens at relatively later times, while the most of the hard particles are emitted from the periphery of the system at early times. In fact (see also [6, 42]), the temperatures in the regions of the maximal emission are quite different for different p_T , they are for pions: $T \approx 75 - 110$ MeV for $p_T = 0.2$ GeV/c and $T \approx 130 - 135$ MeV for $p_T = 1.2$ GeV/c. So, if one uses the generalized Cooper-Frye prescription [6, 42] applied to the *hypersurfaces of the maximal emission*, these hypersurfaces will be different for the different particle momenta and does not correspond to common isotherm [6, 42].

One can see in Fig. 3, the top plots, that at *equal* transverse momentum p_T the maximal emission of kaons happens earlier than pions as one can expect since the kaons interact weaker. At the same time the kaon interferometry radii in Fig. 2 follow approximately to the pion radii, demonstrating the approximate m_T -scaling [43] with deviations to the slightly bigger values than pion radii have. The explanations can be gain from the middle row in Fig. 3 where the comparison is done for the same transverse mass of pions and kaons. Then the maxima of pion and kaon emissions become closer and the majority of kaons leave system even somewhat later than pions at the same m_T , opposite to the comparison at the same p_T . Since in simplest situations the homogeneity lengths for bosons depend on m_T [43], one could say that the approximate m_T -scaling could indicate the similarity of the freeze-out picture for kaons and pions. However, probably, such a conclusion is very approximate since the real structure of the emission processes in A+A collisions is quite complicated as one

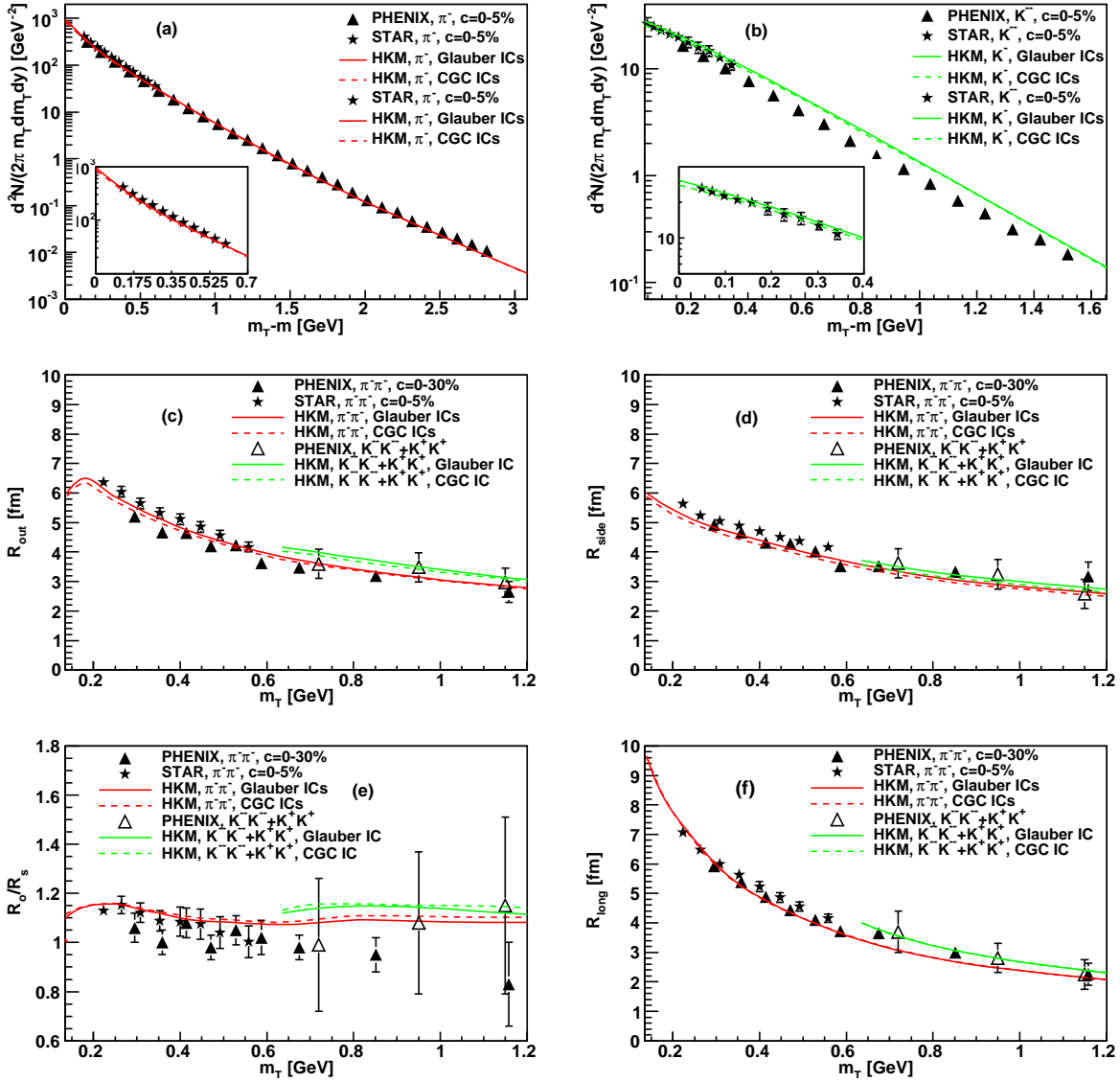


FIG. 2: (Color online) The transverse momentum spectra of (a) negative pions and (b) negative kaons, all calculated in the HKM model. The comparison only with the STAR data are presented in the separate small plots. The interferometry radii: (c) R_{out} , (d) R_{side} , (f) R_{long} and (e) R_{out}/R_{side} ratio for $\pi^-\pi^-$ pairs and mixture of K^-K^- and K^+K^+ pairs. The experimental data are taken from the STAR [44, 45] and PHENIX [46–48] Collaborations.

can see from the details in Fig.3.

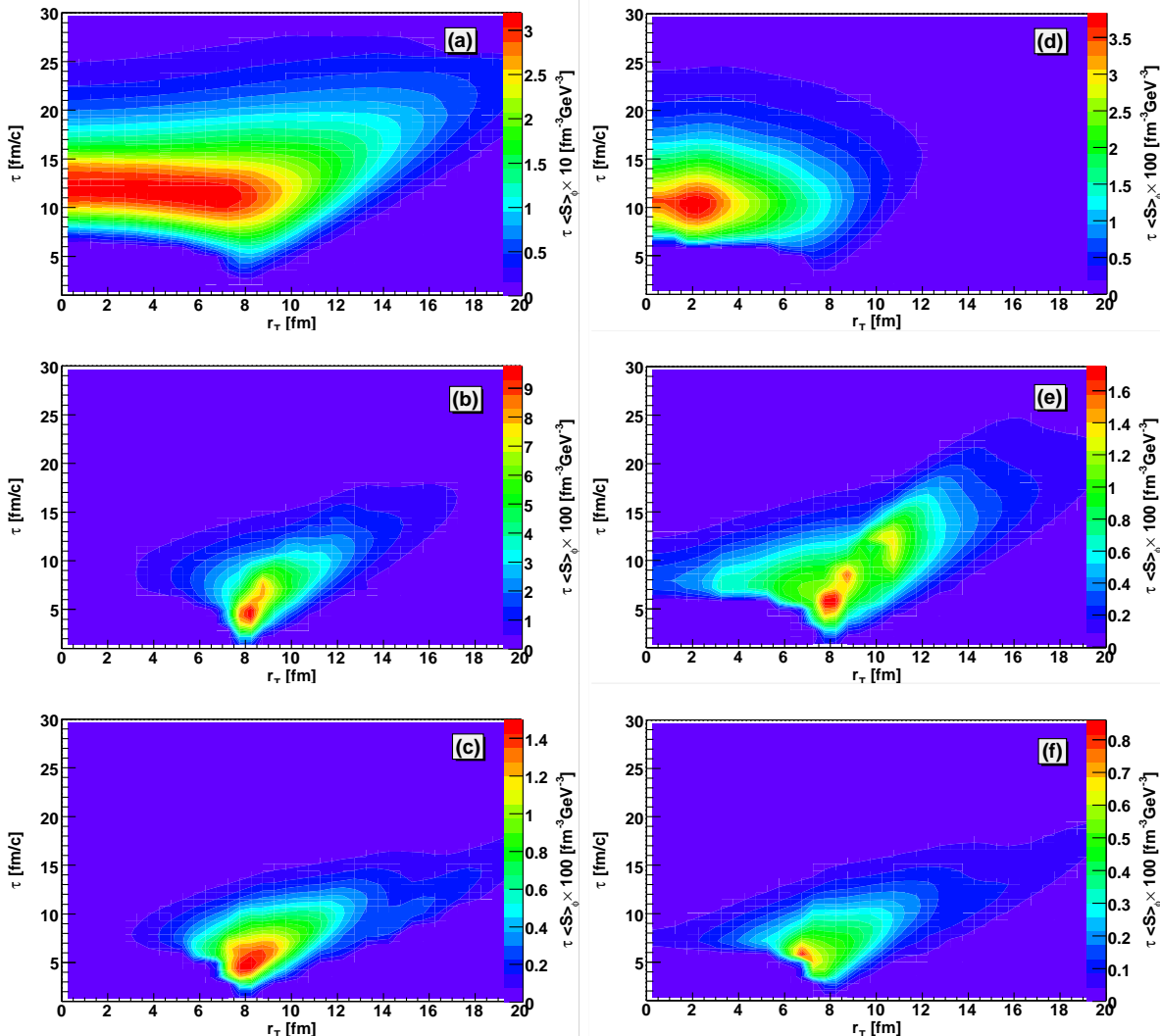


FIG. 3: (Color online) The ϕ_p -integrated emission functions of (a,b,c) negative pions and (d,e,f) negative kaons with different momenta: (a,d) $p_T = 0.2$ GeV, (b) $p_T = 0.85$ GeV, (e) $p_T = 0.7$ GeV, (c,f) $p_T = 1.2$ GeV at the Glauber IC. The values of p_T in the middle row (b,e) correspond to the same transverse mass for pions and kaons $m_T = 0.86$ GeV.

VII. CONCLUSIONS

The hydro-kinetic model [5, 6] is developed for a detailed study of the matter evolution and space-time picture of hadronic emission from rapidly expanding fireballs in $A+A$ collisions. The model allows one to describe the evolution of the QGP as well as the gradually decoupling hadronic fluid - a chemically non-equilibrium matter, where the equation of state is defined at each space-time point and accounts for decays of resonances into the

non-equilibrated medium.

The HKM is applied to restore the initial conditions and space-time picture of the matter evolution in central Au+Au collisions at the top RHIC energy. The analysis, which is based on a detailed reproduction of the pion and kaon momentum spectra and measured femtoscopic scales, demonstrates that basically the pictures of the matter evolution and particle emission are similar at both Glauber and CGC initial conditions (IC) with, however, the different initial maximal energy densities: it is about 20% more for the CGC initial conditions. The initial pre-thermal flow is slightly less for the CGC IC. The main factors, which allows one to describe well simultaneously the spectra and femtosopic scales are: a relatively hard EoS (crossover transition and chemically non-equilibrium composition of hadronic matter), pre-thermal transverse flows developed to thermalization time, an account for an "additional portion" of the transverse flows due to the shear viscosity effect and fluctuation of initial conditions, a correct description of a gradual decay of the non-equilibrium fluid at the late stage of expansion. Then one does not require the too early thermalization time, $\tau_i < 1$ fm/c, to describe the data well. All these factors are included in the presented version of the HKM and it allows one to describe observables with only the two parameters.

An analysis of the emission function at the top RHIC energies demonstrates that the process of decoupling of the fireballs created in Au+Au collision lasts from about 8 to 20 fm/c, more than the half of fireball's total lifetime. The temperatures in the regions of the maximal emission are different at the different transverse momenta of emitting pions: $T \approx 75 - 110$ MeV for $p_T = 0.2$ GeV/c and $T \approx 130 - 135$ MeV for $p_T = 1.2$ GeV/c. A comparison of the pion and kaon emissions at the same transverse mass demonstrates the similarity of the positions of emission maxima, that could point out to the reason for an approximate m_T scaling.

Summary: the advanced HKM tool allows one to describe the process of the fireball evolution and gradual particle liberation in agreement with underlying kinetic equations. Further developments of the hydrokinetic approach and an analysis of the data in non-central A+A collisions will be the subject of a follow-up work.

Acknowledgments

The authors thank S.V. Akkelin for fruitful discussions. The research was carried out within the scope of the EUREA: European Ultra Relativistic Energies Agreement (European Research Group: Heavy ions at ultrarelativistic energies) and is supported by the Fundamental Researches State Fund of Ukraine, Agreement No F33/461-2009 with Ministry for Education and Science of Ukraine. In part it was supported also within the Ukrainian-Russian grant, Agreement No Φ 28/335-2009.

-
- [1] L.D. Landau, *Izv. Akad. Nauk SSSR, Ser. Fiz.* **17**, 51 (1953).
 - [2] Yu.M. Sinyukov, *Nucl.Phys. A* **566**, 589c (1994); Yu.M. Sinyukov, in: *Hot Hadronic Matter: Theory and Experiment*, eds. J. Letessier, H.H. Gutbrod and J. Rafelski (Plenum, New York) 1995, 309.
 - [3] S.A. Bass, A. Dumitru, *Phys. Rev C* **61**, 064909 (2000); D. Teaney, J. Lauret, E.V. Shuryak, *Phys. Rev. Lett.* **86**, 4783 (2001) [arXiv: nucl-th/0110037]; T. Hirano, U. Heinz, D. Kharzeev, R. Lacey, Y. Nara, *Phys. Lett. B* **636**, 299 (2006); C. Nonaka, S.A. Bass, *Phys. Rev. C* **75**, 014902 (2007).
 - [4] W. Florkowski, W. Broniowski, M. Chojnacki, A. Kisiel, *Nucl.Phys. A* **830**, 821c (2009).
 - [5] Yu.M. Sinyukov, S.V. Akkelin, Y. Hama, *Phys. Rev. Lett.* **89**, 052301 (2002).
 - [6] S.V. Akkelin, Y. Hama, Iu.A. Karpenko, and Yu.M. Sinyukov, *Phys. Rev. C* **78**, 034906 (2008).
 - [7] Yu.M. Sinyukov, S.V. Akkelin, Iu.A. Karpenko. *Physics of Atomic Nuclei* **71**, 1619 (2008).
 - [8] K.A. Bugaev, *Phys. Rev. Lett.* **90**, 252301 (2003).
 - [9] Yu.M. Sinyukov, Iu.A. Karpenko, *Nonlinear Phenomena in Complex Systems*, **12**, 496 (2009) [arXiv:0911.4439].
 - [10] D. Teaney, *Phys. Rev. C* **68**, 034913 (2003).
 - [11] Z. Xu, L. Cheng, A. El, K. Gallmeister, C. Greiner, *J. Phys. G: Nucl. Part. Phys.* **36**, 064035 (2009) [arXiv:0812.3839].
 - [12] U. Heinz, *J. Phys. G* **31**, S717 (2005) [arXiv:nucl-th/0512051]; P. Huovinen, P.V. Ruuskanen, *Ann. Rev. Nucl. Part. Sci.* **56**, 163 (2006); T. Hirano, *Nucl. Phys. A* **774**, 531 (2006).
 - [13] Yu.M. Sinyukov, *Acta Phys. Polon. B* **37**, 4333 (2006); M. Gyulassy, Iu.A. Karpenko, A.V.

- Nazarenko, Yu.M. Sinyukov, *Braz. J. Phys.* **37**, 1031 (2007).
- [14] T. Lappi, L. McLerran, *Nucl. Phys. A* **772**, 200 (2006) [arXiv:hep-ph/0602189].
- [15] K. Werner, F.M. Liu, T. Pierog, *Phys. Rev. C* **74**, 044902 (2006) [arXiv:hep-ph/0506232].
- [16] J. Vredevoogd, S. Pratt, arXiv:0810.4325; S. Pratt, arXiv:0903.1469; W. Broniowski, W. Florkowski, M. Chojnacki, A. Kisiel, *Phys.Rev.C* **80**, 034902 (2009).
- [17] Yu.M. Sinyukov, Iu.A. Karpenko, A.V. Nazarenko, *J. Phys. G: Nucl. Part. Phys.* **35**, 104071 (2008).
- [18] Yu.M. Sinyukov, A.V. Nazarenko, Iu.A. Karpenko, *Acta Phys.Polon. B* **40**, 1109 (2009).
- [19] P. F. Kolb, J. Sollfrank, and U. W. Heinz, *Phys. Lett.B* **459** (1999) 667; U. W. Heinz and H. Song, *J. Phys. G* **35** 104126 (2008).
- [20] T. Lappi, *Phys. Lett. B* **643**, 11 (2006) [arXiv:hep-ph/0606207].
- [21] A. Krasnitz, R. Venugopalan, *Phys. Rev. Lett.* **84**, 4309 (2000).
- [22] A. Krasnitz, Y. Nara, R. Venugopalan, *Nucl. Phys.* **A717**, 268 (2003).
- [23] A.Krasnitz *et al.*, *Nucl. Phys.* **A727**, 427 (2003).
- [24] A. Kovner, L. McLerran, H. Weigert, *Phys. Rev.* **D52**, 6231 (1995).
- [25] A. El, Z. Xu, C. Greiner, *Nucl. Phys. A* **806**, 287 (2008) [arXiv:0712.3734]
- [26] E. Wigner, *Phys. Rev.* **40**, 749 (1932).
- [27] M. Hillery, R.F. O'Connell, M.O. Scully, and E.P. Wigner, *Phys. Rep.* **106**, 121 (1984); H.-W. Lee, *Phys. Rep.* **259**, 147 (1995); W.P. Schleich, *Quantum Optics in phase space* (Wiley-VCH, 2001).
- [28] K. Werner, *Phys. Rev. Lett.* **98**, 152301 (2007).
- [29] F. Becattini, J. Manninen *J. Phys. G* **35**, 104013 (2008); J. Manninen, F. Becattini, *Phys. Rev. C* **78**, 054901 (2008);
- [30] A. Andronic, P. Braun-Munzinger, J. Stachel, *Acta Phys.Polon. B* **40**, 1005 (2009).
- [31] M. Laine, Y. Schroder *Phys. Rev. D* **73**, 085009 (2006).
- [32] F. Karsch, PoS CPOD07:026, 2007.
- [33] N.S. Amelin *et al.*, *Phys. Rev. C* **77**, 014903 (2008).
- [34] Iu.A. Karpenko, Yu.M. Sinyukov, *Phys. Lett. B* in press (2010), [arXiv:0912.3457].
- [35] S. Mrowczynski, *Ann.Phys.* **169**, 48 (1986).
- [36] M. Prakash, M. Prakash, R. Venugopalan, and G. Welke, *Phys. Rep.* **227**, 321 (1993).
- [37] S.A. Bass *et al.*, *Prog. Part. Nucl. Phys.* **41**, 225 (1998).

- [38] V. Schneider et al., J. Comput. Phys. **105**, 92 (1993).
- [39] M. Holt, "Numerical methods in fluid dynamics", Springer Series in Comput. Physics (Springer, Berlin, 1977).
- [40] R. Courant, K. Friedrichs and H. Lewy, "On the partial difference equations of mathematical physics", IBM Journal, March 1967, pp. 215-234.
- [41] R.P.G. Andrade, F. Grassi, Y. Hama, T. Kodama, and W.L. Qian, Phys.Rev.Lett.101:112301 (2008).
- [42] Yu.M. Sinyukov, S.V. Akkelin, Iu.A. Karpenko, Y. Hama, Acta Phys.Polon. B **40**, 1025 (2009).
- [43] V.A. Averchenkov, A.N. Makhlin, Yu.M. Sinyukov, Sov. J. Nucl. Phys. **46**, 905 (1987); A. N. Makhlin, Yu. M. Sinyukov, Z. Phys. C **39**, 69 (1988); Yu. M. Sinyukov, Nucl. Phys. A **498**, 151 (1989).
- [44] J. Adams et al. STAR Collaboration, Phys. Rev. Lett. **92**, 112301 (2004).
- [45] J. Adams et al, STAR Collaboration, Phys. Rev. C **71**, 044906 (2004).
- [46] S.S. Adler et al, PHENIX Collaboration, Phys. Rev. C **69**, 034909 (2004).
- [47] S.S. Adler et al, PHENIX Collaboration, Phys. Rev. Lett. **93**, 152302 (2004).
- [48] S. Afanasiev et al., PHENIX Collaboration, Phys. Rev. Lett. **103**, 142301 (2009).